ICAS 2020 SHANGHAI
International Council of the Aeronautical Sciences
32nd Congress of the International Council of the Aeronautical Sciences
September 6-10, 2021
Pudong Shangri-La, Shanghai, China

INFLUENCE OF SHOCK TRAIN ON HEAT FLUX DISTRIBUTION OF A CIRCULAR CONSTANT-AREA ISOLATOR

Xuan Yang[1], Zhong-Wei Wang[1], Yao-Bin Niu[1], He-Yang Miao[1]

[1]College of Aerospace Science and Engineering, National University of Defense Technology, Changsha, Hunan 410073, China

Abstract

The heat flux on isolator wall is investigated numerically. The variation of heat flux is analyzed in detail and the similarities of heat flux profiles between cases under different pressure ratios are summed up. It is found that the heat flux profile can be approximately divided into 3 phases. The similarities of heat flux profiles mainly present in phase Ⅰ and phase Ⅱ, as well as the beginning region of phase Ⅲ. In phase Ⅱ, the wall heat flux increases firstly about 9.4% and then decreases about 21.5%, namely from 0.93MW/m^2 to 0.73MW/m^2 when pressure ratio is 4. The obvious increase of heat flux in phase Ⅱ is mainly due to the greatly increasing fluid temperature near the wall, which is caused by the extrusion process between the incoming flow and the vortex near the wall at the starting location of shock train. The following sharp decrease of heat flux is mainly due to the decreasing fluid temperature and thicker velocity boundary layer when the flow field is away from the extrusion interface. Remarkably, the location of sharply decreased heat flux in phase Ⅱ is closer to the entrance of isolator with higher pressure ratio.

Keywords: Isolator; Heat flux; Pressure ratio; Shock train; Numerical simulation

1. Introduction

With the development of science and technology, people prefer aircraft with higher velocity. Hypersonic vehicle is a novel type of aircraft with five times or higher speed of sound in the atmosphere [1-2]. Due to the perfect performance under high flying Mach number, the scramjet has become the ideal propulsion equipment of the hypersonic aircraft [3]. To prevent the unstable high pressure in combustion chamber influencing the compression progress of the incoming flow in the inlet [4-6], the isolator is designed in scramjet. Due to the high flight Mach number, however, the total temperature of the incoming air in isolator can be up to 1800K [7] and the isolator wall will bear severe heat load. Meanwhile, due to the high pressure in combustion chamber, the shock train, which has significant effect on the heat transfer process, is formed in the isolator. Therefore, it is necessary to analyze the influence of flow field on wall heat flux for better design of isolator's thermal protection system.

The shock train in isolator has been studied a lot for many years. Some researchers investigated the influence of back pressure, namely the outlet pressure of isolator, on the location of shock train in isolator [7-9]. Huang et al. [7] studied the evolution of the shock train in circular isolator and found that the location of shock train will be closer to the entrance with the increase of back pressure. Meanwhile, rectangular isolators with different ratio of length to height and divergence angle were also investigated and the influence of back pressure on the location of shock train was analyzed [9]. The length of shock train is also needed to be considered in the design of isolator. Waltrup et al. [10] and Bement et al. [11] investigated the length of shock train in isolator, and some formulas were established. Lin et al. [12] compared the flow field in rectangular isolator and circular isolator. They found that the length of shock train in circular isolator is shorter than that in rectangular isolator, which means that the ability of the circular isolator to resist the back pressure is better than that of rectangular isolator. The transient characteristics of flow field in isolator has also been analyzed. Xiong et al. [13-15] carried out experimental and numerical study on the self-excited oscillation of the shock train in a rectangular isolator. Su [16] investigated the control of

pseudo-shock oscillation by using unsteady Reynolds averaged Navier-Stokes simulations.
It is remarkably to note that the flow structure in isolator can be influenced by many factors. Su et al. [17] and Lin [18] studied the relationship between the wall temperature and the location of shock train. They found that the location of shock train will be closer to the entrance with higher wall temperature. Wang et al. [19] studied the flow field in isolator with asymmetric incoming airflow and found that the increase of the asymmetry will lead to the increase of the shock train length. He et al. [20] studied the influence of combustion chamber on shock train structure in isolator, and they found that, for the circular constant-area isolator, there is no obvious difference between shock train structures calculated with or without considering the combustion progress of fuel.
At present, the heat transfer process in isolator has seldom been investigated. Dai et al. [21] studied the heat transfer process in isolator numerically. They found that the wall heat flux increases gradually near the outlet of isolator and they tend to believe that the increase of heat flux is caused by the department of boundary layer from the wall due to the influence of shock train. However, the variation of heat flux along the isolator has not been systematically analyzed in detail. Remarkably, the wall heat flux may change sharply near the location of the shock train due to the local complex flow field, which cannot be neglected when we design the thermal protection system of isolator and is needed to be further analyzed.
In this paper, the flow and heat transfer process in isolator is investigated numerically. Meanwhile, the influence of flow field, especially that near the location of shock train, on the variation of wall heat flux is analyzed in detail.

2. Physical model and numerical method

2.1 Physical model

As shown in Figure 1, the length of circular constant-area isolator L is 715mm and the radiator of isolator R is 65mm. The wall thickness is neglected.

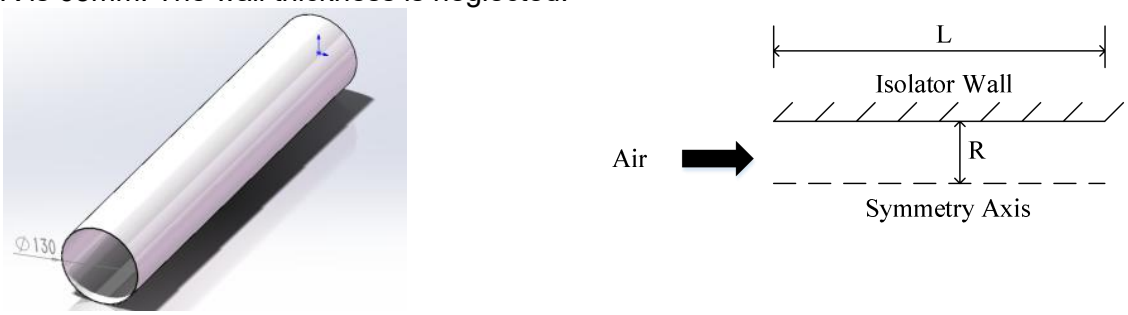

（a）three-dimensional schematic of isolator　　（b）two-dimensional schematic of isolator

Figure 1 – Physical model of isolator

2.2 Numerical method

2.2.1 Simulation methodology

Two-dimensional Reynolds-averaged Navier-Stokes equations are used to simulate the flow field and heat transfer process in isolator. The transport equations governing the turbulent flow in Fluent 16.1 are shown in *Eqs. (1)-(3)*.
Continuity equation:

$$\frac{\partial \rho}{\partial t}+\frac{\partial\left(\rho u_i\right)}{\partial x_i}=0 \tag{1}$$

Momentum equation:

$$\frac{\partial\left(\rho u_i\right)}{\partial t}+\frac{\partial}{\partial x_j}\left(\rho u_j u_i\right)=\rho f_i-\frac{\partial P}{\partial x_i}+\frac{\partial}{\partial x_j}\left[\mu\left(\frac{\partial u_i}{\partial x_j}+\frac{\partial u_j}{\partial x_i}\right)\right] \tag{2}$$

Energy equation:

$$\frac{\partial(\rho E)}{\partial t}+\frac{\partial}{\partial x_j}\left[u_i(\rho E+p)\right]=\frac{\partial}{\partial x_j}\left[\left(k+\frac{Cp\mu_t}{Pr_t}\right)\frac{\partial T}{\partial x_j}+u_t\left(\mu_{eff}\left(\frac{\partial u_i}{\partial x_j}+\frac{\partial u_j}{\partial x_i}\right)\right)\delta_{ij}\right]+S_h \tag{3}$$

The turbulence model used in this paper is Re-Normalization Group (RNG) k-ε turbulence model. The transport equations are shown in *Eqs. (4)-(5)*.

$$\frac{\partial(\rho k)}{\partial t}+\frac{\partial}{\partial x_i}\left[\rho k u_i\right]=\frac{\partial}{\partial x_j}\left(\alpha_k\mu_{eff}\frac{\partial k}{\partial x_j}\right)+G_k+G_b-\rho\varepsilon-Y_M+S_K \tag{4}$$

$$\frac{\partial(\rho\varepsilon)}{\partial t}+\frac{\partial}{\partial x_j}\left(\rho\varepsilon u_i\right)=\frac{\partial}{\partial x_j}\left(\alpha_\varepsilon\mu_{eff}\frac{\partial\varepsilon}{\partial x_j}\right)+C_{1\varepsilon}\frac{\varepsilon}{k}\left(G_k+C_{3\varepsilon}G_b\right)-C_{2\varepsilon}\rho\frac{\varepsilon^2}{k}-R_\varepsilon+S_\varepsilon \tag{5}$$

The density-based solver in FLUENT 16.1 is used to solve the governing equations and turbulence model. Meanwhile, the enhanced wall treatment is adopted.

2.2.2 Boundary condition

Pressure inlet boundary condition and pressure outlet boundary condition are used in this paper. The inlet total pressure is set to be 2.0265MPa, the inlet static pressure is set to be 118606Pa and the total temperature is 1800K. The pressure ratio P_b, which is defined as the ratio of outlet static pressure to inlet static pressure, is set to be 3, 4 and 5. The wall temperature is set to be 900K to simulate the heat transfer process in isolator. The material of isolator wall is steel.

2.2.3 Validation of numerical methods

The Kawatsu's experimental data [22] is used to validate the numerical methods. The Mach number is 2.3, the total pressure P_0 is 100kPa and the pressure ratio is 3.8. Pressure outlet boundary condition and pressure inlet boundary condition are used. As shown in Figure 2, the variation of simulated pressure profile matches well with that measured in experiments.

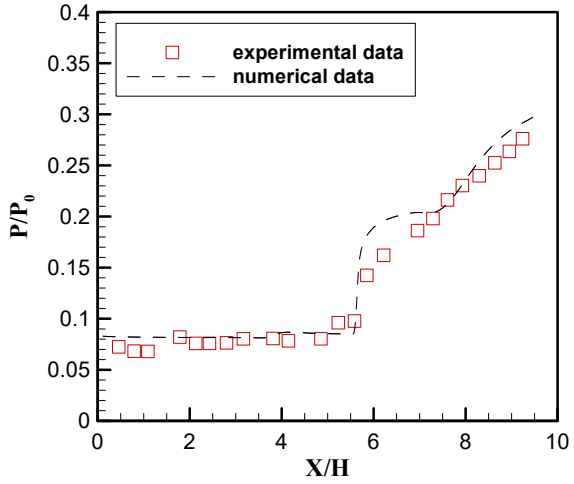

Figure 2 – Static pressure on isolator wall

2.2.4 Mesh independence validation

The structured mesh is used in this paper. The first layer of grids near the wall surface is refined, namely 2×10^{-6} m, and y^+ is smaller than 1. Three different meshes are designed, namely the coarse mesh (480×120), the medium mesh (720×180) and the refined mesh (1040×260).

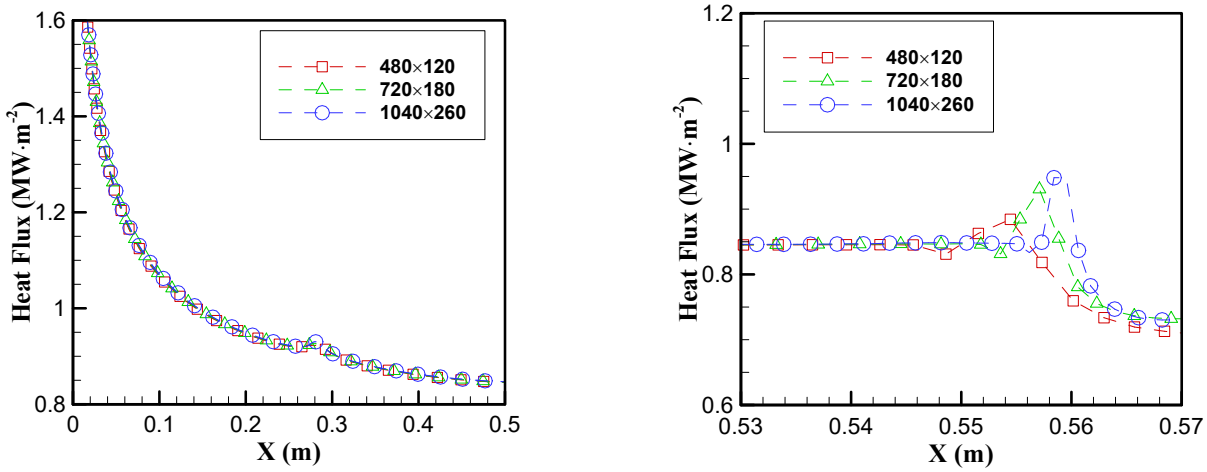

(a) wall heat flux before the oblique shock wave (b) wall heat flux near the oblique shock wave

Figure 3 – Heat flux profiles under different meshes

As shown in Figure 3(a), the heat flux profiles before the oblique shock wave have no obvious difference between different meshes. In Figure 3(b), the variation of heat flux profiles under different meshes near the oblique shock wave are similar. The heat flux peak is about 0.885MW/m^2, 0.930MW/m^2 and 0.948MW/m^2 in these 3 cases with different meshes, respectively. The error of heat flux peak between the coarse mesh case and medium mesh case is about 5.1%. Meanwhile, the error between medium mesh case and refined mesh case is only about 1.9%. Considering the cost of calculation, the medium mesh is chosen for latter calculation.

3. Results and discussion

The heat flux on isolator wall is calculated under different pressure ratios. The variation of heat flux profiles, as well as the relationship between the heat flux and flow field, are summed up and some regular results are found.

3.1 The flow structure in isolator

The flow fields under different pressure ratios are nearly the same except the vortex structure near the wall. As shown in Figure 4, due to the high pressure in combustion chamber, the revised flow is presented at the outlet of isolator and the vortex is formed near the wall. Meanwhile, due to the extrusion between the vortex and incoming flow, the oblique shock wave is formed accordingly. With the increase of pressure ratio, the location of the shock train is closer to the inlet of isolator.

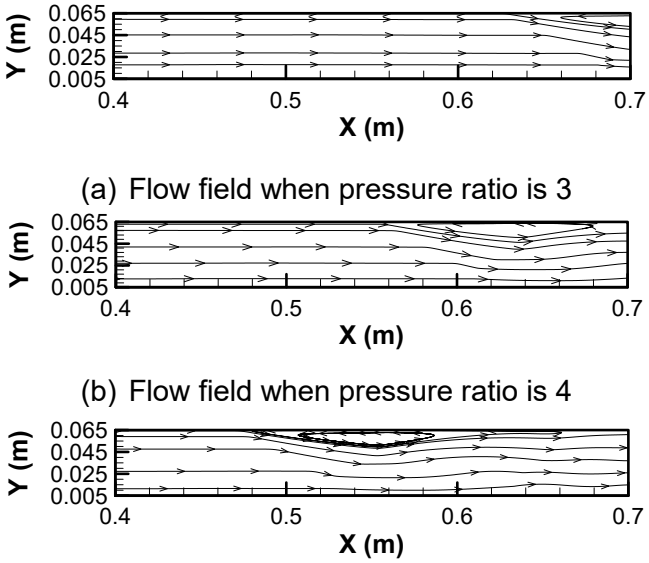

(a) Flow field when pressure ratio is 3

(b) Flow field when pressure ratio is 4

(c) Flow field when pressure ratio is 5

Figure 4 – Flow fields in isolator under different pressure ratios

3.2 The heat flux on isolator wall under different pressure ratios

3.2.1 The characteristics of heat flux on isolator wall

The variation of heat flux on isolator wall is shown in Figure 5. For better description, the heat flux profile can be approximately divided into 3 phases as follows. In phase Ⅰ, the heat flux decreases gradually. The heat flux profiles under different pressures are nearly the same and are about 0.85MW/m^2 at the end of phase Ⅰ, which means that the outlet pressure has little influence on the heat flux in phase Ⅰ. In phase Ⅱ, firstly, the heat flux peak is presented. When the pressure ratio is 4, the increase of heat flux is about 9.4%, from 0.85MW/m^2 to 0.93MW/m^2. Following the peak, the heat flux decreases sharply about 21.5%, namely from 0.93MW/m^2 to 0.73MW/m^2. In phase Ⅲ, the heat flux profiles are quite different due to the influence of different vortex in the wall-adjacent region. However, the heat flux profiles all present an increasing trend at the beginning of this region. In conclusion, the similarities among the heat flux profiles under different pressure ratios mainly present in the first and second phase, as well as the region near the beginning of phase Ⅲ.

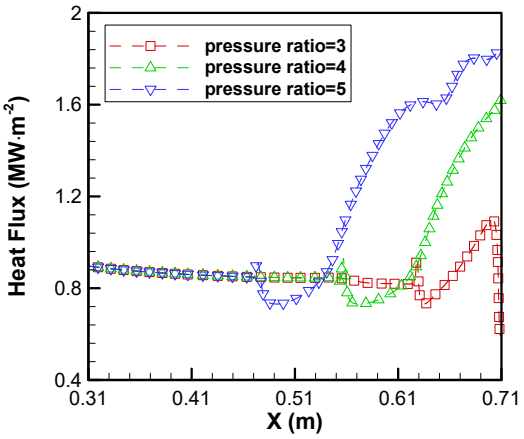

Figure 5 – Heat flux on isolator wall under different pressure ratios

3.2.2 Comparison between the pressure and heat flux on isolator wall

The heat flux profiles, namely the dashed lines, and pressure profiles on isolator wall under different pressure ratios are shown in Figure 6. The relationship between them is analyzed in detail. Remarkably, it is interesting to note that the heat flux changes sharply at the location where pressure profiles have a steep growth. Meanwhile, the location where the heat flux decreases sharply moves toward the entrance of isolator with the increase of pressure ratio.

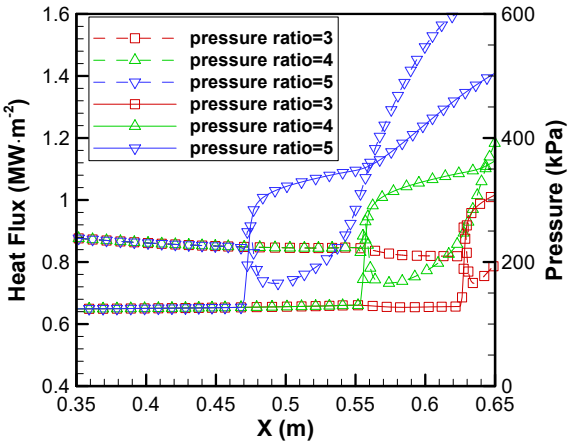

Figure 6 – Heat flux and pressure on isolator under different pressure ratios

The steep growth of wall pressure usually means that the shock train wave is formed. As shown in Figure 7, the starting location of shock train wave matches well with that of sharply changed heat flux profiles and pressure profiles, which means that phase Ⅱ is in the region near the starting location of shock train. Accordingly, phase Ⅰ is in the region before the location of the shock train.

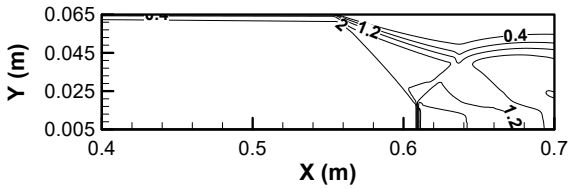

Figure 7 – Mach number counter in isolator

3.3 Variation of heat flux on isolator wall

In this section, the variation of heat flux is analyzed in detail. As discussed above, the variation of heat flux under different pressure ratios is similar in phase Ⅰ and phase Ⅱ, as well as the beginning region of phase Ⅲ. Due to these similarities under different pressure ratios, only the simulated results are presented when pressure ratio is 4.

3.3.1 Decrease of heat flux in phase Ⅰ

The decreasing tendency of heat flux in phase Ⅰ is analyzed in detail. As shown in Figure 8, the temperature of fluid in the wall-adjacent region along the isolator decreases gradually due to the cooling effect of low temperature wall and the temperature gradient also decreases, which will inhibit the local heat transfer process. As shown in Figure 9, due to the decreasing fluid temperature near the wall, the thermal boundary layer becomes thicker along the isolator in phase Ⅰ.

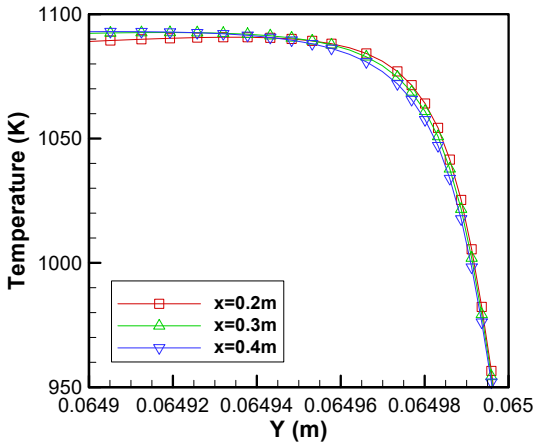

Figure 8 – Temperature profiles along the isolator in phase Ⅰ

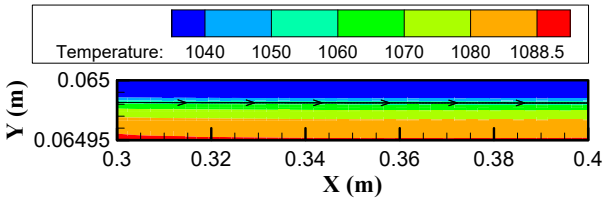

Figure 9 – Flow field near the wall in phase Ⅰ

Meanwhile, as shown in Figure 10, along the isolator, the fluid velocity near the wall decreases gradually due to the wall friction and the velocity boundary layer becomes thicker.

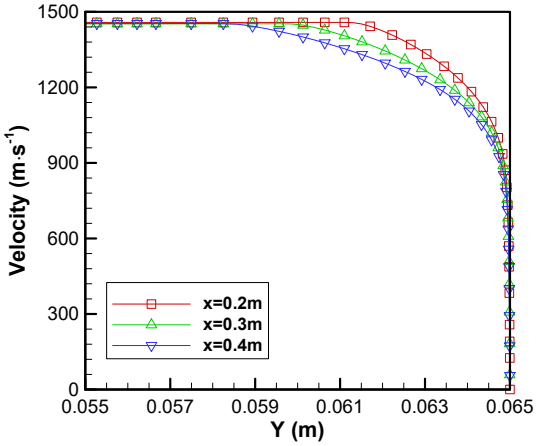

Figure 10 – Velocity profiles before the location of the oblique shock wave

Accordingly, due to the decreasing fluid velocity and temperature, as well as the thicker velocity

and temperature boundary layer, the heat transfer in the wall-adjacent region is inhibited and the heat flux on isolator wall decreases gradually.

3.3.2 Heat flux on isolator wall in phase Ⅱ

The variation of heat flux along the isolator in phase Ⅱ is non-monotonic. As shown in Figure 11, the heat flux near the starting location of shock train fluctuates obviously and can be approximately divided into 2 parts. In part 1, the heat flux increases and then decreases sharply in part 2.

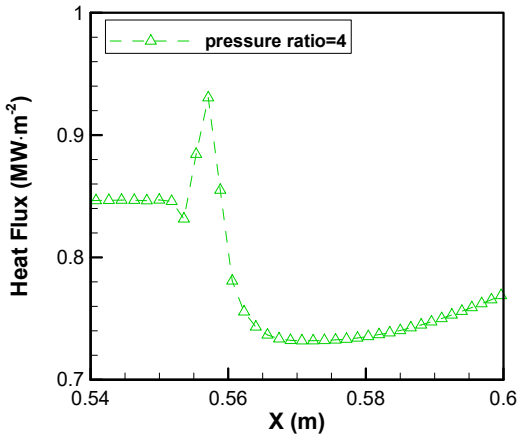

Figure 11 – Variation of heat flux in phase Ⅱ

The variation of heat flux in these 2 parts is analyzed in detail.

In part 1, as shown in Figure 12, the fluid temperature peak increases sharply about 180K along the isolator from x=0.553m to x=0.557m. Since the high temperature fluid near the wall is the heat source, the sharp increase of fluid temperature peak will accordingly lead to the increase of wall heat flux.

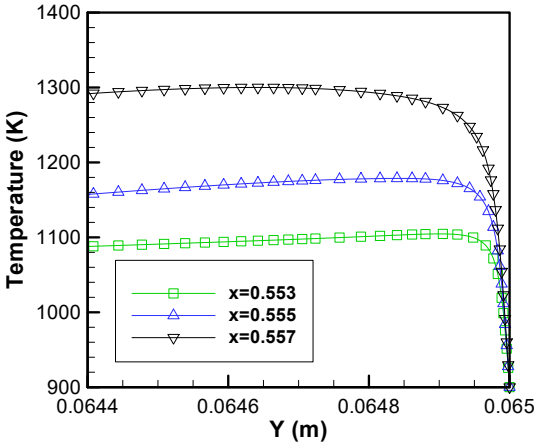

Figure 12 – Temperature profiles along the isolator in part 1

Meanwhile, as shown in Figure 13, the region with sharp increase of fluid temperature is near the location where vortex near the wall is formed. Hence, it seems that due to the high back pressure, the incoming flow extrudes with the vortex near the wall and the shock train is formed. Due to the extrusion process between the incoming flow and the vortex, the static temperature of incoming flow increases obviously along the isolator, which will lead to the increasing heat source and accordingly the increasing wall heat flux in part 1.

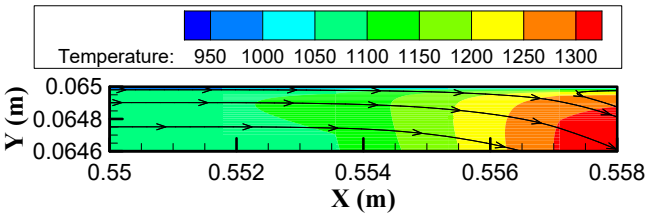

Figure 13 – Flow field and temperature counter in part 1

In part 2, as is shown in Figure 14, the fluid temperature in wall-adjacent region decreases gradually along the isolator, which will lead to the decreasing temperature gradient and inhibited heat transfer. Meanwhile, as shown in Figure 15, the boundary layer becomes thicker along the isolator in part 2, which will also lead to inhibited heat transfer.

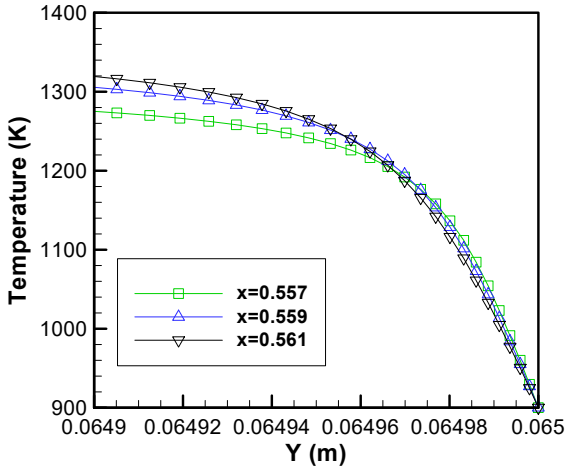

Figure 14 – Temperature profiles along the isolator in part 2

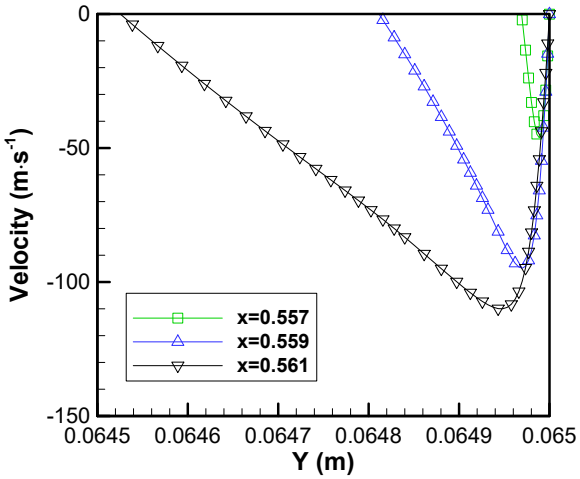

Figure 15 – Velocity profiles along the isolator in part 2

The decreasing fluid temperature gradient and thicker velocity boundary layer along the isolator in part 2, which will accordingly lead to the decreasing wall heat flux, is mainly caused by the fact that the fluid near the wall is far away from the extrusion interface. As shown in Figure 16, in part 2, the fluid near the wall is the vortex region, which means that the isolator wall heat flux is directly influenced by the vortex. Due to the extrusion process caused by the incoming flow, the velocity boundary layer becomes thinner along the flow direction of the vortex near the wall, which is opposite to the positive direction of x coordinate. Hence, the velocity distribution of fluid in the wall-adjacent region shown in Figure 15 is formed.

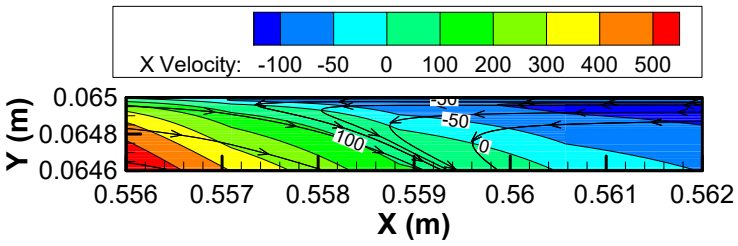

Figure 16 – Velocity profiles along the isolator in part 2

3.3.3 Heat flux on isolator wall in phase Ⅲ

In phase Ⅲ, as shown in Figure 5, the heat flux profiles are quite different among the calculated cases due to the influence of different vortex in the wall-adjacent region. However, the heat flux profiles all present an increasing trend at the beginning region of phase Ⅲ. In this section, the increasing trend of heat flux is further analyzed.

As shown in Figure 17, the fluid temperature near the wall increases gradually along the isolator, which will finally lead to the increasing temperature gradient along the isolator. As shown in Figure

18, the flow direction of vortex in phase Ⅲ is opposite to the positive direction of x coordinate. Accordingly, the fluid is cooled by the low temperature wall along the flow direction.

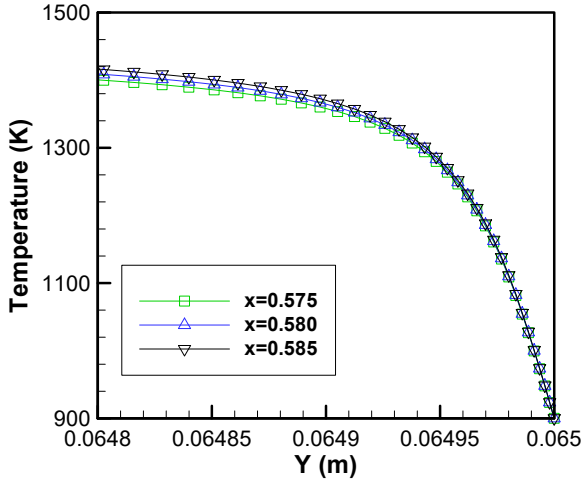

Figure 17 – Temperature profiles along the isolator in phase Ⅲ

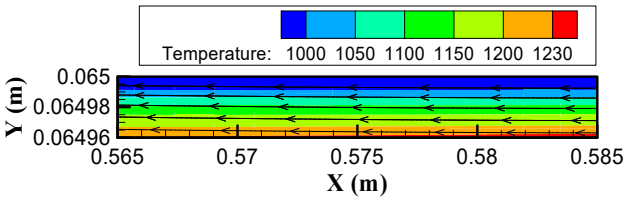

Figure 18 – Flow field and temperature counter in phase Ⅲ

Meanwhile, as shown in Figure 19, the fluid velocity in vortex near the wall increases gradually along the wall, which is due to the influence of extrusion process near the starting location of shock train, as well as the effect of wall friction. The increasing fluid temperature and velocity in phase Ⅲ will finally lead to the increasing wall heat flux.

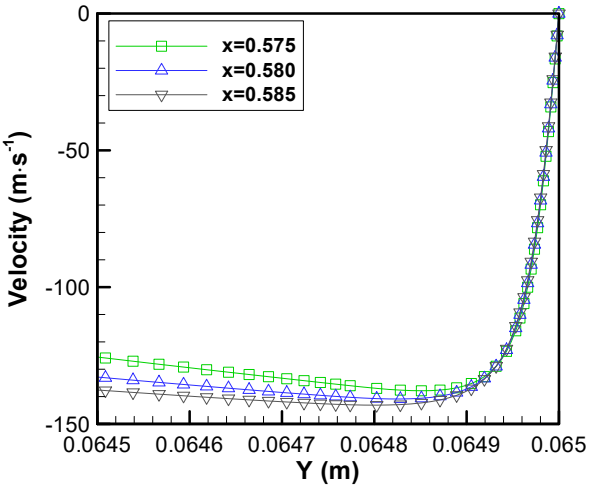

Figure 19 – Fluid velocity in phase Ⅲ

4. Conclusions

The flow field and heat transfer process in isolator is numerically studied in this paper under different pressure ratios and the variation of heat flux on isolator wall is analyzed in detail. The conclusions are obtained as follows.

(1) The heat flux profiles under different pressure ratios can be divided into 3 phases. Phase Ⅰ is namely the region before the starting location of shock train. Phase Ⅱ is around the starting location of shock train. The similarities among these heat flux profiles mainly present in phase Ⅰ and phase Ⅱ, as well as the beginning region of phase Ⅲ.

(2) In phase Ⅰ, the heat flux profiles under different pressure ratios are nearly the same. Meanwhile, the heat flux in phase Ⅰ decreases gradually and is close to 0.85MW/m^2 near the starting location of shock train. The decrease of heat flux is mainly due to the thicker velocity boundary layer and lower fluid temperature near the wall along the isolator.

(3) In phase Ⅱ, the heat flux profiles can be further divided into 2 parts. In part 1, the heat flux

profiles mainly show an increasing tendency from 0.85MW/m^2 to 0.93MW/m^2, which is about 9.4% when pressure ration is 4. The increase of heat flux is mainly caused by the fact that at the starting location of shock train, the incoming flow extrudes with the vortex in wall-adjacent region, which will lead to the obviously increasing fluid temperature peak near the wall. since the high temperature fluid near the wall is the heat source in isolator, the obviously increasing fluid temperature peak will lead to the increasing heat source in isolator accordingly. In part 2, the heat flux decreases sharply about 21.5%, namely from 0.93MW/m^2 to 0.73MW/m^2 when pressure ration is 4, due to the decreasing fluid temperature near the wall and thicker velocity boundary layer as the region is away from the extrusion interface.

(4) In phase Ⅲ, the heat flux is mainly influenced by the vortex in the wall-adjacent region. Accordingly, the heat flux profiles under different pressures are different. However, at the beginning of phase Ⅲ, the heat flux profiles all show an increasing tendency, which is mainly caused by the increasing fluid temperature and fluid velocity in near wall region.

References

[1] Jones RA, Huber PW. Toward scramjet aircraft. *Astronautics and Aeronautics*, Vol. 27, pp 38-48,1978.

[2] Voland RT, Huebner LD, McClinton CR. X-43A hypersonic vehicle technology development. *Acta Astronautica*, Vol. 59, pp 181-191, 2006.

[3] Tetlow PW, Doolan C. Comparison of hydrogen and hydrocarbon-fueled scramjet engines for obtical insertion. *Journal of Spacecraft and Rockets*, Vol. 44, pp 365-373, 2007.

[4] Curran ET, Heiser WH and Pratt DT. Fluid Phenomena in Scramjet Combustion Systems. *Annual Review of Fluid Mechanics*, Vol. 28, pp 323–360, 1996.

[5] Heiser WH, Pratt DT, Daley DH and Mehta UB. *Hypersonic Air Breathing Propulsion*. 1st edition, American Institute of Aeronautics & Astronautics, 1994.

[6] Emami S, Trexler CA, Auslender AH and Weidner JP. Experimental Investigation of Inlet-Combustor Isolators for a Dual Mode Scramjet at a Mach Number of 4. *NASA*, 1995, Report No.TP-3502.

[7] Huang W, Luo SB, Wang Y, Wang ZG. Research of evolution of shock train in scramjet isolator. *Machinery Design and Manufacture*, Vol. 5, pp 201-203, 2010. (in chinese)

[8] Huang W, Wang ZG, Pourkashanian M, Ma L, Ingham DB, Luo SB, Lei J and Liu J. Numerical investigation on the shock wave transition in a three-dimensional scramjet isolator. *Acta Astronautica*, Vol. 68, pp 1669-1675, 2011.

[9] Jin L, Wu XY, Luo SB, Wang ZG. Influence of back pressure on location of shock train in isolator. *Journal of propulsion technology*, Vol. 29, No. 1, pp 54-57, 2008. (in chinese)

[10] Waltrup PJ, Billing FS. Structure of shock waves in cylindrical ducts. *AIAA Journal*, Vol. 11, No. 10, pp 1404-1408, 1973.

[11] Bement DA, Stevens JR and Thompson MW. Measured operating characteristic of a rectangular combustor/inlet isolator. *26th Joint Propulsion Conference*, Orlando, Vol. 1, 2221, pp 1-8, 1990.

[12] Lin P. Geometric effects on precombustion shock train in constant area isolators. *29th Joint Propulsion Conference and Exhibit*, Monterey, Vol. 1, 1838, pp 1-12, 1993.

[13] Xiong B, Wang ZG, Fan XQ and Li TJ. Characteristics of Forced Normal Shock-Train Oscillation in Isolator. *Journal of Propulsion Technology*, Vol. 38, No. 1, pp 1-7, 2017. (in chinese)

[14] Xiong B, Wang ZG and Fan X Q. Response of shock train to high-frequency fluctuating backpressure in an isolator. *Journal of Propulsion and Power*, Vol. 33, pp 1520-1528, 2017.

[15] Fan X Q, Xiong B, Wang Y and Yuan T. Experimental study on the self-excited oscillation and the forced oscillation of shock train in a rectangular isolator. *21st AIAA International Space Planes and Hypersonics Technologies Conference*, Xiamen, Vol. 1, 2115, pp 1-11, 2017.

[16] Su WY, Chen Y, Zhang FR and Tang PP. Control of pseudo-shock oscillation in scramjet inlet-isolator using periodical excitation. *Acta Astronautica*, 143, 2017.

[17] Su WY, Wang H, Chen Y and Zhang KY. Effects of wall temperature on pseudo-shock oscillations in isolator. *Journal of Aerospace Power*, Vol. 32, No. 7, pp 1605-1612, 2017.

[18] Lin KC, Tam CJ, Eklund DR, Jackson K and Jackson T. Effects of temperature and heat transfer on shock train structures inside constant-area isolators. *44th AIAA Aerospace Sciences Meeting and Exhibit*, Vol. 1, 817, pp 1-14, 2006.

[19] Wang CP, Zhang KY and Cheng KM. Investigation of flow in isolators under asymmetric incoming airflow. *Journal of propulsion technology*, Vol. 27, No. 5, pp 436-440, 2006. (in chinese)

[20] He C, Xing JW, Xiao BG and Liu WX. Influence of back pressure on shock train structure in isolator. *Journal of Aerospace power*, Vol. 31, No. 5, pp 1242-1251,2016.

[21]Dai JF, Pan Y and Yang HA. Effects of back pressure on heat transfer of constant round area isolator. *Journal of thermal science and technology*, Vol. 15, No. 3, pp 185-189, 2016. (in chinese)

[22]Kawatsu K, Koike S, Kumasaka T, Masuya G and Takita K. Pseudo-shock wave produced by back pressure in straight and diverging rectangular Ducts. *13th International Space Planes and Hypersonics Systems and Technologies Conference*, Vol. 1, 2585, pp 1-11, 2005.

Contact Author Email Address

mailto: xuanyang_2018@163.com

Copyright Statement